Title
Massively parallel delivery of large cargo into mammalian cells with light pulses

Journal
Nature Methods, 12(5)

ISSN
1548-7091

Authors
Wu, YC
Wu, TH
Clemens, DL
et al.

Publication Date
2015-04-29

DOI
10.1038/nmeth.3357

Peer reviewed

Massively parallel delivery of large cargo into mammalian cells with light pulses

Yi-Chien Wu[1], Ting-Hsiang Wu[1,2], Daniel L Clemens[3], Bai-Yu Lee[3], Ximiao Wen[1], Marcus A Horwitz[3], Michael A Teitell[2,4,5] & Pei-Yu Chiou[1,4,5]

We report a high-throughput platform for delivering large cargo elements into 100,000 cells in 1 min. Our biophotonic laser-assisted surgery tool (BLAST) generates an array of microcavitation bubbles that explode in response to laser pulsing, forming pores in adjacent cell membranes through which cargo is gently driven by pressurized flow. The platform delivers large items including bacteria, enzymes, antibodies and nanoparticles into diverse cell types with high efficiency and cell viability. We used this platform to explore the intracellular lifestyle of *Francisella novicida* and discovered that the *iglC* gene is unexpectedly required for intracellular replication even after phagosome escape into the cell cytosol.

The efficient delivery of large cargo elements such as functional nanoparticles, subcellular organelles and microbial pathogens would be useful for cellular engineering, imaging and sensing, as well as the study of normal and disease states and intracellular pathogenesis. However, reliable methodologies for introducing large cargo into mammalian cells at high throughput are currently lacking[1]. Biological approaches such as viruses can provide high transfer efficiency[2,3] but are restricted to kilobase-sized nucleic acids. Chemical methods that utilize lipids[4], cationic polymers[5] or insoluble precipitates vary in delivery efficiency, are highly cell-type dependent and frequently show undesirable endosome trapping of delivered cargo.

Most physical approaches can bypass endocytosis, and the delivery typically involves two steps: (i) disruption of the plasma membrane to create transient pores and (ii) cargo delivery across transient pores before they reseal. To create transient pores, electroporation uses electrostatic forces to disrupt cell membranes[6–8]; sonoporation[9,10] generates acoustic pressure to trigger cavitation bubbles with strong fluid flows to induce membrane permeability; optoporation[11–13] uses nonlinear optical absorption triggered by a short laser pulse to break down cell membranes; and microfluidic channels[14] use narrow structures to squeeze cell membranes.

These mechanisms are limited to small-cargo delivery because they rely on thermal diffusion for cargo crossing at transient membrane pores. Slowly diffusing large cargo has little chance to transit pores before they reseal. Nanochannel electroporation[8] can induce convective injection by electrophoresis, but it is suitable only for nanosized cargo. Molecules adhering onto nanomechanical pillars[15] can be introduced into cells directly. However, sharp tips coated with large cargo may lose the ability to penetrate cell membranes. Micropipette-based approaches provide active pressure to drive large cargo into the cell cytosol[16–19]. These methods, however, are low throughput and may suffer from complications, such as clogging or traumatic cell lysis, as cargo size increases beyond ~500 nm.

To overcome the bottleneck for large-cargo delivery, we developed the massively parallel photothermal BLAST platform to deliver up to micrometer-sized cargo into ~100,000 cells in 1 min, providing throughput five orders of magnitude higher than that of prior microcapillary-based approaches[19]. We successfully delivered a wide range of cargo types including live bacteria, enzymes, antibodies and functional nanoparticles into a variety of cell lines, including three types of primary cells (human peripheral blood monocyte–derived macrophages (PB-MDMs), primary normal human dermal fibroblasts (NHDFs) and human primary renal proximal tubule epithelial cells (RPTECs)) and one cancer cell line (HeLa), at high efficiency and high cell viability. We have also shown that BLAST delivers cargo directly into the cell cytosol, avoiding cargo entrapment in endosomes and maintaining cargo functionality after delivery.

RESULTS

The design and operating principle of BLAST

The BLAST platform consists of a silicon chip with a thin, porous SiO_2 membrane on top providing an array of micrometer-wide, trans-film holes whose side walls are asymmetrically coated with crescent-shaped titanium thin films (**Fig. 1a**). Underneath the SiO_2 membrane is an array of short, vertical silicon channels mechanically supporting the fragile membrane as well as providing fluid passage for cargo delivery (see **Supplementary Fig. 1** for detailed fabrication process). The procedure for cargo delivery on a BLAST

[1]Department of Mechanical and Aerospace Engineering, University of California at Los Angeles, Los Angeles, California, USA. [2]Department of Pathology and Laboratory Medicine, David Geffen School of Medicine, University of California at Los Angeles, Los Angeles, California, USA. [3]Division of Infectious Diseases, Department of Medicine, David Geffen School of Medicine, University of California at Los Angeles, Los Angeles, California, USA. [4]Department of Bioengineering, University of California at Los Angeles, Los Angeles, California, USA. [5]California NanoSystems Institute (CNSI), University of California at Los Angeles, Los Angeles, California, USA. Correspondence should be addressed to P.-Y.C. (pychiou@seas.ucla.edu) or M.A.T. (mteitell@ucla.edu).

RECEIVED 25 AUGUST 2014; ACCEPTED 9 MARCH 2015; PUBLISHED ONLINE 6 APRIL 2015; DOI:10.1038/NMETH.3357

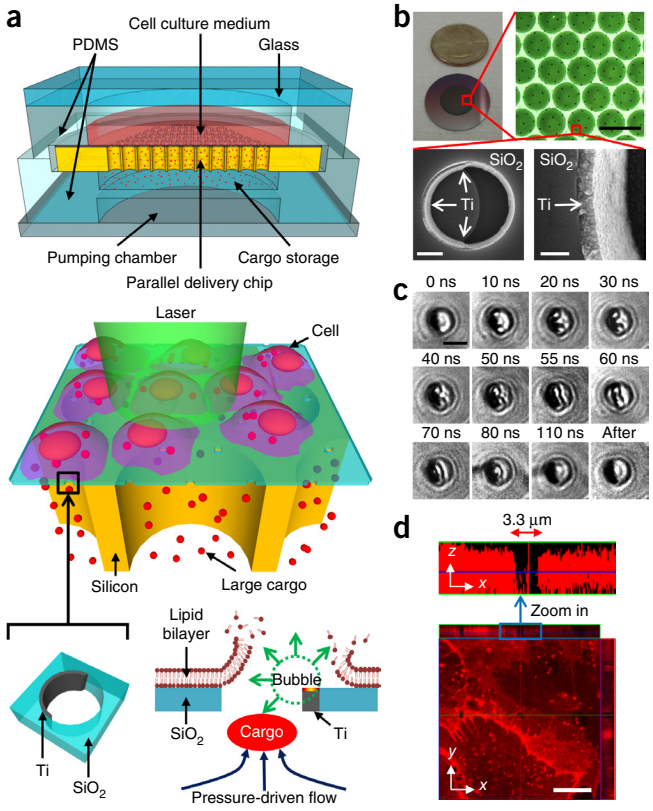

Figure 1 | Design and operation of the BLAST large-cargo delivery platform. (**a**) The platform consists of an array of trans-membrane holes patterned on a 1.5-μm-thick SiO_2 film. Crescent-shaped titanium films are asymmetrically coated on the side walls of these holes to harvest laser pulse energy. Rapid pulsed laser scanning of the active photothermal region on the chip triggers cavitation bubbles in all holes that disrupt contacting cell membranes. After membrane opening, an external pressure source is applied to deform the bottom flexible poly(dimethylsiloxane) (PDMS) storage chamber to push cargo into the cytosol of cells via these transient membrane pores. (**b**) Images of a BLAST chip for delivery. Scanning electron microscopy images (bottom) show a 100-nm-thick titanium film coated on the inner side wall of a 3-μm hole on the SiO_2 membrane. Scale bars, 100 μm (top right), 1 μm (bottom left) and 200 nm (bottom right). (**c**) Time-resolved images capture rapidly expanding cavitation bubbles triggered in a hole from 10 to 110 ns after laser pulsing. At 10–50 ns, two bubbles form and enlarge at the upper and lower poles of the hole; at 55 ns, the bubbles coalesce; and by 110 ns, the bubbles collapse. Scale bar, 3 μm. (**d**) Confocal *z*-axis scanning images show that the cell membrane of a fixed cell on the platform is disrupted and reveal a micrometer-sized pore after laser pulsing. Scale bar, 20 μm.

platform is as follows. (i) Cells are cultured or made to adhere on a silicon chip. (ii) The chip is assembled with a microliter chamber loaded with the cargo to be delivered. (iii) A nanosecond-pulse laser scans rapidly across the entire chip to generate membrane pores in cells contacting the titanium films, and immediately thereafter the elastic chamber is pressurized to deliver cargo into cells through these transient pores (**Supplementary Note**). Laser pulsing and cargo pumping (step iii) take 10 s. BLAST delivers cargo into cells in a batch mode. Each batch can deliver cargo into 100,000 cells with the current chip area (1 cm^2). For delivery of cargo to more cells, as many chips as desired can be prepared and steps ii and iii repeated. Each batch delivery takes about 1 min.

Mechanism of opening transient cell-membrane pores

BLAST uses laser energy harvested by the metallic titanium thin films in each trans-film hole (**Fig. 1b**) to induce rapid heating and vaporization of adjacent water layers, triggering cavitation bubbles[20–24]. The bubbles in each SiO_2 hole initiate at the two tips of the crescent-shaped titanium film, where hotspots are located. Local electric field enhancement occurs near the tips owing to the lightning-rod effect, and bubble size is highly dependent upon laser fluence (**Supplementary Fig. 2**). Scanning the chip with laser pulses triggers cavitation bubbles that grow, coalesce and collapse within 110 ns (**Fig. 1c**). This rapid bubble 'explosion' induces strong fluid flows that can disrupt an adjacent plasma membrane[19]. Confocal fluorescence imaging of pores formed in the plasma membrane of chemically fixed cells on the platform revealed that cell membrane cutting by BLAST is highly localized (**Fig. 1d**).

Delivery efficiency and membrane resealing time

Cell viability and membrane opening efficiency by BLAST depends on the SiO_2 hole density (higher densities generate more transient pores per cell) and laser pulse energy. We experimentally determined the optimal conditions for high membrane-opening efficiency with high cell viability (>90%) for HeLa cells as approximately one or two holes per cell with a laser fluence of 55 mJ/cm^2 (**Fig. 2a–d**).

Cell membrane resealing starts immediately after transient pores are generated[25]. Large-cargo delivery is challenging because these transient pores shrink quickly, thereby impeding the diffusion of large cargo through them—a relatively slow process. Therefore, we initiated active rather than diffusion-based cargo delivery in the time before membrane resealing. To measure the transient opening time frame for large-cargo delivery, we delivered a micrometer-sized bacterium, GFP-expressing *F. novicida*, into HeLa cells at various delay time intervals between laser pulsing and active fluid pumping. Cells were incubated for 12 h at 37 °C after delivery to allow the GFP-expressing bacteria to replicate extensively in the cytosol; we then counted the cells completely filled with green fluorescent bacteria. As expected, delivery efficiency decreased with increasing delay time. With no delay, the average delivery efficiency across the entire chip was ~58%, whereas with a 10-s delay, the efficiency dropped to ~20% (**Fig. 2e**). The delivery of small cargo can tolerate a longer delay time. For example, high efficiency delivery could be maintained for up to several minutes for membrane-impermeable calcein dye (**Fig. 2f**), a result suggesting that a micrometer-sized pore opened by a cavitation bubble quickly shrinks to exclude the delivery of large cargo but remains permeable to small molecules. Complete membrane resealing takes longer than 10 min. Of note, the 40–50% average efficiency for delivering intracellular bacteria was partially due to the slow laser scanning. In our current setup, it took about 10 s to scan the entire 1-cm^2 chip. Many cells in the initially scanned regions had shrunk their pores by the time the pressured delivery was applied, thus reducing bacterial delivery efficiency.

BLAST delivery also worked well for primary mammalian cells. FITC-dextran (40 kDa) dye was delivered into NHDFs, PB-MDMs and RPTECs, and we incubated the cells on the platform for 3 d to check viability and proliferation. All three primary cell lines retained high cell viability (>90%) 3 d after delivery (**Fig. 2g**). The delivery efficiencies for NHDFs and RPTECs were higher than 90%. PB-MDMs approached only 60% efficiency, likely because of their smaller size and reduced contact area with the platform compared

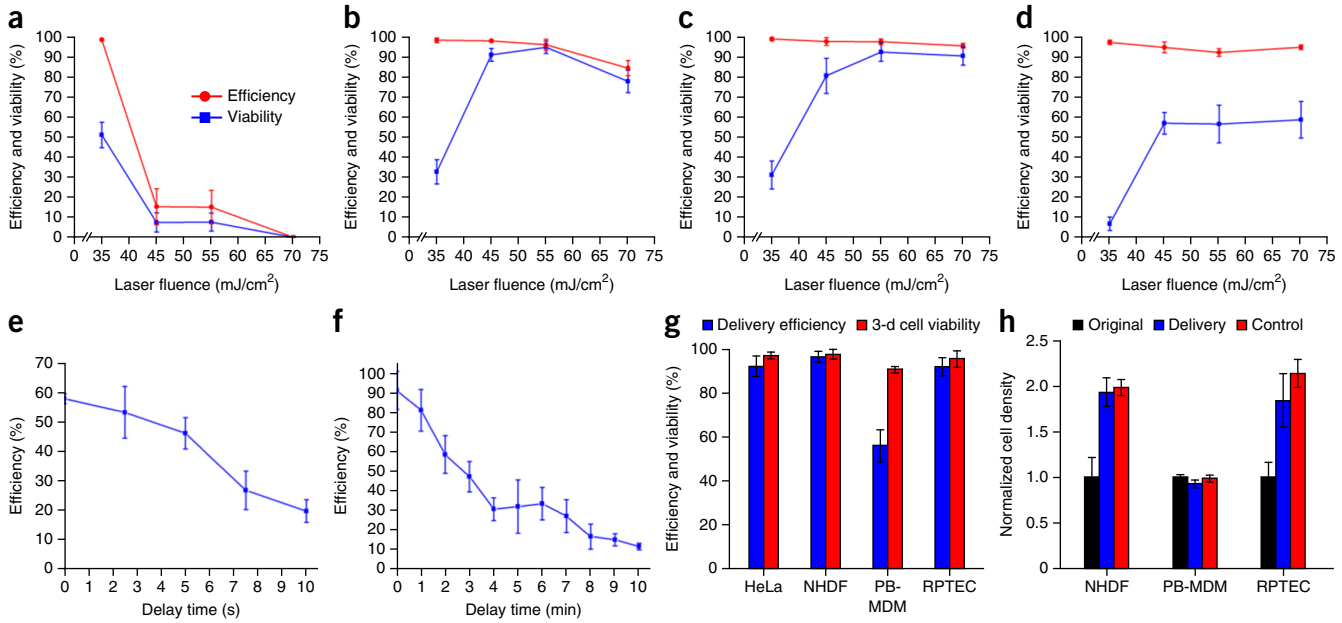

Figure 2 | Cell membrane pore-opening efficiency, cell viability and pore resealing time. (**a**–**d**) Cargo delivery efficiency and cell viability as a function of laser fluence and hole density on the chip, with densities of 1.15 (**a**), 0.28 (**b**), 0.18 (**c**) or 0.12 holes per 10 μm^2 (**d**). Pore-opening efficiency is determined by calcein dye (622 Da) uptake for HeLa cells. Error bars, s.d. (n = 2,031, 1,483, 1,601 and 1,975 cells for **a**–**d**, respectively; cell density, 1,138 cells/mm^2). (**e**,**f**) Characterization of the transient window for large-cargo and small-molecule delivery. (**e**) Delivery efficiency of *F. novicida* bacteria into HeLa cells at different delay times between laser pulsing and fluid pumping. Error bars, s.d. (n = 1,926, 2,062, 2,335, 2,406 and 2,106 cells for 0, 2.5, 5, 7.5 and 10 s, respectively). (**f**) Delivery efficiency of calcein at different delay times. The cell membrane pores remained permeable for longer than 10 min for small-molecule delivery. Error bars, s.d. (n = 5,891 cells for all tests). (**g**) FITC-dextran (40 kDa) delivery efficiency and 3-day cell viability for different kinds of primary mammalian cells. Error bars, s.d. (n = 2,030, 1,512, 1,464 and 532 for HeLa cells, NHDFs, PB-MDMs and RPTECs, respectively). (**h**) Densities of primary cells with delivered FITC-dextran (40 kDa) cultured on chips for 3 d compared with the original cell densities. Control cells were seeded on chips at the same time without laser pulsing and fluid pumping. Error bars, s.d. (n = 3,062, 3,017 and 1,149 for NHDFs; PB-MDMs and RPTECs, respectively; initial cell densities were 265, 534 and 98 cells/mm^2, respectively).

to much larger NHDF and RPTEC cells (**Supplementary Fig. 3**). We quantified the proliferation of primary cells after cargo delivery by cell density determinations for cells with or without (control, no laser pulsing or fluid pumping) FITC-dextran delivery and found that BLAST delivery did not affect cell growth (**Fig. 2h**). PB-MDMs, which are terminally differentiated cells that do not divide, maintained their original cell density.

In addition to live intracellular bacteria, a variety of other large cargo items, including antibodies, magnetic beads and micrometer-sized polystyrene beads have also been successfully delivered into cells using BLAST (**Supplementary Fig. 4a–c**). To study the effect of cargo size on delivery efficiency, we delivered five different sizes of polystyrene beads (20 nm, 200 nm, 500 nm, 1 μm and 2 μm). The efficiency decreased as cargo size increased, from 93% for 20-nm beads to 62% for 2-μm beads; cell viability in all cases was maintained above 90% (**Supplementary Fig. 4d**). Multiple payloads can be delivered at the same time. In fact, combinatorial delivery is one major advantage of BLAST, as it offers less size-diffusion variance by providing active pressure–driven flows during delivery (**Supplementary Fig. 4e,f**). Evaluation of stress levels of HeLa cells after BLAST delivery showed no major increase in heat-shock *HSPA6* gene expression, a general cell stress sensor (**Supplementary Fig. 5**). All cell and cargo types, delivery efficiencies and cell viabilities are summarized in **Supplementary Table 1**.

Direct delivery into the cytosol bypasses endocytosis

To confirm that BLAST delivers biologically active and undamaged cargo directly into the cell cytosol, we delivered the bacterial enzyme β-lactamase (29 kDa) by BLAST into NHDFs and evaluated its delivery and functional activity by incubating the cells with the esterified β-lactamase substrate CCF4-AM. When CCF4-AM enters the cytosol, endogenous esterases convert it to CCF4, which can be detected by fluorescence resonance energy transfer (FRET). Excitation of CCF4 at a wavelength of 408 nm leads to efficient FRET and emission of green fluorescence at 530 nm. Bacterial β-lactamase that was delivered by BLAST into the cell cytosol cleaved CCF4 into two separate fluorophores, causing the FRET effect to be lost, with the emission fluorescence changing from green to blue at 460 nm. CCF4-loaded cells at 5 h after β-lactamase delivery are shown (**Fig. 3**). NHDFs into which more enzyme was delivered showed a higher blue-to-green fluorescence intensity ratio (**Supplementary Fig. 6**). This result shows that the enzyme remains functional in the cytosol after BLAST delivery.

We also delivered an escape-incompetent strain of *Listeria monocytogenes* deficient in listeriolysin O and phospholipase C[26] into NHDFs (strains are described in **Supplementary Table 2**). This *L. monocytogenes* mutant is well established as being unable to escape its vacuole to recruit actin and thereby form actin comet tails in the cytosol[26]. Formation of actin tails (visualized by red fluorescent rhodamine-phalloidin staining) by these bacteria after BLAST delivery is strong direct evidence that they were delivered directly into the cell cytosol and remained alive and metabolically active (**Fig. 4a**). In the absence of laser pulsing, these escape-incompetent bacteria were taken up poorly and never formed actin tails (**Fig. 4b,c**). Because NHDFs are not phagocytic, uptake

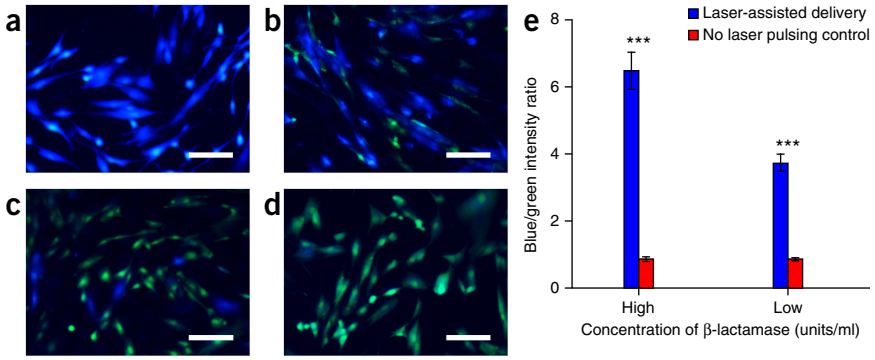

Figure 3 | BLAST-delivered β-lactamase enzyme is functional inside NHDFs. (**a**–**d**) β-lactamase at 50 units/ml (**a**,**c**) or 1 unit/ml (**b**,**d**) in PBS were delivered into NHDFs using BLAST under the condition of fluid pumping but with (**a**,**b**) or without (**c**,**d**) laser pulsing. Scale bars, 100 µm. (**e**) Blue and green fluorescent intensities for all four groups were measured 5 h after β-lactamase delivery. A higher blue-to-green fluorescence ratio means more β-lactamase was delivered into cells and remained functional, and was thus able to cleave CCF4 molecules. Error bars, s.d. (n = 976, 577, 1,005 and 353 cells for 50 units/ml delivery, 50 units/ml control, 1 unit/ml delivery and 1 unit/ml control, respectively; ***P < 0.0001, Student's t-test). The experiment was conducted three times with the same results.

of the bacteria by NHDFs in the absence of laser pulsing was extremely inefficient, and as a result, considerably more bacteria were observed in the laser pulsed cells than in non-laser-pulsed control cells (**Fig. 4**; $P < 0.0001$ by Student's t-test for difference in the number of bacteria delivered with versus without laser pulsing). We obtained the same results after BLAST delivery of these bacteria into HeLa cells (data not shown) and have confirmed that they are unable to form actin tails after phagocytic uptake and endolysosomal entrapment by THP-1 macrophages (**Supplementary Fig. 7**).

Study of intracellular lifestyle of a pathogen using BLAST

BLAST enables massively parallel, highly efficient and nearly simultaneous delivery of large cargo into mammalian cells under uniform physiological conditions. This feature allows for reliable statistical analysis of delivered cargo and their interactions with cells over time. Here, as an example, we used BLAST to examine the role of *iglC*, a gene within the *Francisella* pathogenicity island (FPI), in intracellular replication of *Francisella*.

Francisella is a highly virulent Gram-negative facultative intracellular bacterium that causes a fatal zoonotic disease, tularemia. *Francisella* subverts host-cell trafficking by preventing phagolysosomal fusion and escapes into the host-cell cytosol, where it replicates[27]. Essential to its virulence and its capacity to escape into the cytosol and replicate intracellularly is a cluster of 17 genes, the FPI, thought to encode a type 6 secretion system[28–30]. Disruption of almost any of the FPI genes prevents phagosome escape and intracellular replication[31]. Because vacuolar escape precedes and appears to be required for intracellular bacterial replication of *Francisella*, it has been impossible to determine whether the FPI is required only for vacuolar permeabilization and bacterial escape into the cytosol or is additionally required for intracytosolic activities such as replication following escape.

Three strains of *F. novicida*—the wild type, a Δ*iglC* mutant in which the *iglC* gene has been deleted, and a Δ*iglC* mutant complemented with the *iglC* gene—were delivered into HeLa cells (**Supplementary Fig. 8**). HeLa cells are nonphagocytic and inefficiently internalize *F. novicida* on their own, but using BLAST, we could deliver the *F. novicida* strains directly into the cell cytosol. After the HeLa cells recovered, they were harvested from the BLAST platform for study of bacterial intracellular trafficking and multiplication over time. Bacterial replication at 22 h after these three strains were delivered into HeLa cells is shown in fluorescence images (**Fig. 5a**–**c**).

We used a modification of the differential digitonin permeabilization assay[32] to identify cytosolic versus vacuolar bacteria, confirming extensive cytosolic localization of the bacteria (**Fig. 5d** and **Supplementary Fig. 9**). Approximately 50–60% of these three types of *F. novicida* delivered on the platform were found in the cytosol 1 h after delivery, a result suggesting that 40–50% of bacteria were repackaged into vacuoles. The wild-type and *iglC*-complemented *F. novicida* showed a higher ratio in the cytosol with increasing incubation time ($P < 0.001$ and $P < 0.01$, respectively, two-way ANOVA with Bonferroni post-test correction). We assayed bacterial intracellular growth by counting the number of bacteria in HeLa cells over time (**Fig. 5e**). The *Francisella* wild-type strain replicated extensively within the cytosol as evidenced by large areas of green fluorescence within the HeLa cells at 22 h (**Fig. 5a**,**e**), whereas, unexpectedly, the *Francisella* with a deleted

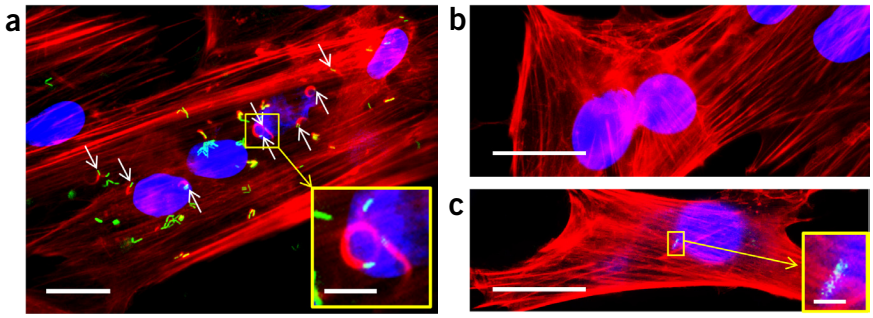

Figure 4 | Escape-incompetent *L. monocytogenes*, deficient in listeriolysin O and broad-range phospholipase C, nucleate actin after BLAST delivery directly into the cytosol of NHDFs. *L. monocytogenes-GFP Δhly ΔplcB* (green), strain 10403S, was delivered by BLAST with laser pulsing into the cytosol of NHDFs (**a**) or, as a sham control, in the absence of laser pulsing (**b**,**c**). Nuclei, stained with DAPI, fluoresce blue; and F-actin, stained by phalloidin-rhodamine, fluoresces red. A higher magnification of a green fluorescent bacterium and its actin comet tail after BLAST delivery with laser pulsing is shown (**a**, inset). In the absence of laser pulsing, intracellular bacteria are rare and comet tails are not seen (**b**,**c**, inset). Scale bars, 20 µm (full images in **a**–**c**), 5 µm (**a** inset) and 2 µm (**c** inset). The experiment was conducted twice with the same results each time.

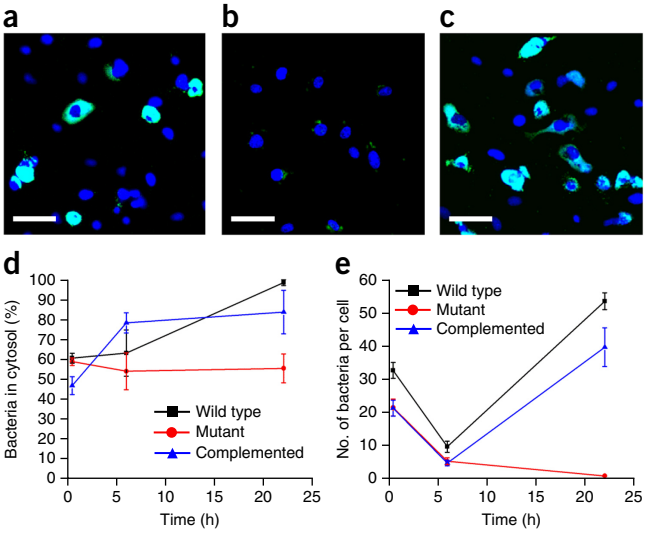

Figure 5 | The *iglC* gene of *F. novicida* is required for intracellular multiplication after cytosolic delivery. GFP-expressing *F. novicida* wild type (**a**), Δ*iglC* mutant (**b**) and Δ*iglC* mutant complemented with *iglC* (**c**) in the cytosol of HeLa cells at 22 h after delivery. The bacteria fluoresce green, and cell nuclei are stained blue with DAPI. Scale bars, 50 µm. (**d**) Percentage of bacteria in the cytosol was assessed by the differential digitonin permeabilization assay. Error bars, s.d. (n = 712 cells for all tests). (**e**) Growth of *F. novicida* wild type, Δ*iglC* mutant and complemented Δ*iglC* mutant in HeLa cells after cytosolic delivery. Error bars, s.e.m. (n = at least 7 randomly selected microscopic fields of view per data point with at least 74 cells evaluated per data point). The experiment was conducted twice with similar results.

iglC gene[33] was unable to replicate intracellularly even after direct delivery into the cytosol (**Fig. 5b,e**).

Complementation of the *iglC* gene from a plasmid restored the capacity of the Δ*iglC* mutant to multiply within HeLa cells after cytosolic delivery (**Fig. 5c,e**), indicating that *iglC* is required for bacterial cytosolic replication even after vacuolar escape. Indeed, growth curves revealed that numbers of Δ*iglC* mutant bacteria per HeLa cell decrease over time, suggesting that host defense mechanisms of HeLa cells were able to kill and destroy the mutant bacteria (**Fig. 5e**). In contrast, wild-type bacteria, which replicate intracellularly, appeared immune to these host defenses. At 22 h, the numbers of wild-type and complemented bacteria per cell were both significantly greater than the number of mutant bacteria per cell ($P < 0.001$, two-way ANOVA with Bonferroni post-test correction). Previously, the *iglC* gene has been known to be critically important in phagosome permeabilization, but our data indicate that it is also required for *Francisella* cytosolic replication even after phagosome escape.

DISCUSSION

The potential applications of BLAST are broad. In addition to the delivery of small and medium cargo elements such as quantum dots, gold nanospheres, functional enzymes and combinations of DNA and RNA, BLAST may enable new fields by providing a high-throughput tool to deliver ultralarge cargo into cells, which was not previously possible. Examples include delivery of whole mitochondria for study of diseases of mutant mitochondrial DNA, whole chromosomes for cell engineering and intracellular pathogens to study the mechanisms of pathogenesis.

BLAST provides a physical approach for reliably puncturing mammalian cell membranes in contact with metallic nanostructured thin films using short-laser-pulse illumination. Our data show that a similar pulse energy efficiently opens pores in the plasma membranes of a variety of mammalian cells and that pressured flow can drive virtually any type of particle into cells without aggregation or endosomal entrapment. The massively parallel and near-simultaneous nature of delivery means that an experiment using a single chip can produce sufficient data for statistical analysis.

The ability to deliver bacteria into 100,000 host cells at one time will enable researchers to follow large populations of infected cells over time in order to study phenomena such as bacterial localization and intracellular multiplication. Although the bacterial delivery experiment was intended only to demonstrate the utility of BLAST, we unexpectedly discovered that the *iglC* gene is required for cytosolic replication after phagosome escape. Such a study would be nearly impossible using conventional pipette-based delivery approaches because they do not provide the throughput required for reliable statistical analysis, and rapid events do not benefit from the synchronization that comes from simultaneous infection.

METHODS

Methods and any associated references are available in the online version of the paper.

Note: Any Supplementary Information and Source Data files are available in the online version of the paper.

ACKNOWLEDGMENTS

This work was supported by a University of California Discovery Biotechnology Award (178517), US National Institutes of Health grants AI065359, GM114188 and EB014456, and by NanoCav, LLC. This work was also funded by US National Science Foundation grant CBET-1404080. The authors thank K. Niazi and S. Rabizadeh for helpful discussions and support, D.A. Portnoy (University of California, Berkeley) for providing the *L. monocytogenes* strain DP-L2318, D.M. Monack (Stanford University) for the *F. novicida* ΔFPI strain, K.E. Klose (University of Texas at San Antonio) for the *F. novicida* U112 strain, F.E. Nano (University of Victoria) for the codon-optimized superfolder *gfp* and J.S. Hong (University of California, Los Angeles) for the stress gene assay.

AUTHOR CONTRIBUTIONS

Y.-C.W., T.-H.W. and P.-Y.C. had the idea for the platform. Y.-C.W. designed and fabricated the BLAST device. T.-H.W. built the experimental setup. Y.-C.W., T.-H.W., D.L.C. and B.-Y.L. performed the experiments and analyzed the data. B.-Y.L. prepared mutant and complemented *Francisella* strains. X.W. ran the numerical simulations. P.-Y.C., M.A.T. and M.A.H. advised on experiments, data analysis and paper writing. All authors discussed the experimental results and wrote the paper.

COMPETING FINANCIAL INTERESTS

The authors declare no competing financial interests.

1. Rusk, N. Seamless delivery. *Nat. Methods* **8**, 44 (2011).
2. Naldini, L. *et al.* *In vivo* gene delivery and stable transduction of nondividing cells by a lentiviral vector. *Science* **272**, 263–267 (1996).
3. Akin, D. *et al.* Bacteria-mediated delivery of nanoparticles and cargo into cells. *Nat. Nanotechnol.* **2**, 441–449 (2007).
4. Felgner, P.L. *et al.* Lipofection: a highly efficient, lipid-mediated DNA-transfection procedure. *Proc. Natl. Acad. Sci. USA* **84**, 7413–7417 (1987).
5. De Smedt, S.C., Demeester, J. & Hennink, W.E. Cationic polymer based gene delivery systems. *Pharm. Res.* **17**, 113–126 (2000).
6. Somiari, S. *et al.* Theory and *in vivo* application of electroporative gene delivery. *Mol. Ther.* **2**, 178–187 (2000).

7. Guignet, E.G. & Meyer, T. Suspended-drop electroporation for high-throughput delivery of biomolecules into cells. *Nat. Methods* **5**, 393–395 (2008).
8. Boukany, P.E. *et al.* Nanochannel electroporation delivers precise amounts of biomolecules into living cells. *Nat. Nanotechnol.* **6**, 747–754 (2011).
9. Kim, H.J., Greenleaf, J.F., Kinnick, R.R., Bronk, J.T. & Bolander, M.E. Ultrasound-mediated transfection of mammalian cells. *Hum. Gene Ther.* **7**, 1339–1346 (1996).
10. Mitragotri, S. Healing sound: the use of ultrasound in drug delivery and other therapeutic applications. *Nat. Rev. Drug Discov.* **4**, 255–260 (2005).
11. Tirlapur, U.K. & König, K. Cell biology: targeted transfection by femtosecond laser. *Nature* **418**, 290–291 (2002).
12. Tao, W., Wilkinson, J., Stanbridge, E.J. & Berns, M.W. Direct gene transfer into human cultured cells facilitated by laser micropuncture of the cell membrane. *Proc. Natl. Acad. Sci. USA* **84**, 4180–4184 (1987).
13. Chakravarty, P., Qian, W., El-Sayed, M.A. & Prausnitz, M.R. Delivery of molecules into cells using carbon nanoparticles activated by femtos laser pulses. *Nat. Nanotechnol.* **5**, 607–611 (2010).
14. Sharei, A. *et al.* A vector-free microfluidic platform for intracellular delivery. *Proc. Natl. Acad. Sci. USA* **110**, 2082–2087 (2013).
15. Shalek, A.K. *et al.* Vertical silicon nanowires as a universal platform for delivering biomolecules into living cells. *Proc. Natl. Acad. Sci. USA* **107**, 1870–1875 (2010).
16. Capecchi, M.R. High efficiency transformation by direct microinjection of DNA into cultured mammalian cells. *Cell* **22**, 479–488 (1980).
17. Zhang, Y. & Yu, L.-C. Microinjection as a tool of mechanical delivery. *Curr. Opin. Biotechnol.* **19**, 506–510 (2008).
18. Hurtig, J. & Orwar, O. Injection and transport of bacteria in nanotube-vesicle networks. *Soft Matter* **4**, 1515–1520 (2008).
19. Wu, T.-H. *et al.* Photothermal nanoblade for large cargo delivery into mammalian cells. *Anal. Chem.* **83**, 1321–1327 (2011).
20. Hartland, G.V. Optical studies of dynamics in noble metal nanostructures. *Chem. Rev.* **111**, 3858–3887 (2011).
21. Link, S. & El-Sayed, M.A. Spectral properties and relaxation dynamics of surface plasmon electronic oscillations in gold and silver nanodots and nanorods. *J. Phys. Chem. B* **103**, 8410–8426 (1999).
22. Kotaidis, V., Dahmen, C., von Plessen, G., Springer, F. & Plech, A. Excitation of nanoscale vapor bubbles at the surface of gold nanoparticles in water. *J. Chem. Phys.* **124**, 184702 (2006).
23. Lukianova-Hleb, E. *et al.* Plasmonic nanobubbles as transient vapor nanobubbles generated around plasmonic nanoparticles. *ACS Nano* **4**, 2109–2123 (2010).
24. Furlani, E.P., Karampelas, I.H. & Xie, Q. Analysis of pulsed laser plasmon-assisted photothermal heating and bubble generation at the nanoscale. *Lab Chip* **12**, 3707–3719 (2012).
25. Yamane, D. *et al.* Electrical impedance monitoring of photothermal porated mammalian cells. *J. Lab. Autom.* **19**, 50–59 (2014).
26. Marquis, H., Doshi, V. & Portnoy, D.A. The broad-range phospholipase C and a metalloprotease mediate listeriolysin O-independent escape of *Listeria monocytogenes* from a primary vacuole in human epithelial cells. *Infect. Immun.* **63**, 4531–4534 (1995).
27. Clemens, D.L., Lee, B.-Y. & Horwitz, M.A. Virulent and avirulent strains of *Francisella tularensis* prevent acidification and maturation of their phagosomes and escape into the cytoplasm in human macrophages. *Infect. Immun.* **72**, 3204–3217 (2004).
28. Nano, F.E. & Schmerk, C. The *Francisella* pathogenicity island. *Ann. NY Acad. Sci.* **1105**, 122–137 (2007).
29. Barker, J.R. *et al.* The *Francisella tularensis* pathogenicity island encodes a secretion system that is required for phagosome escape and virulence. *Mol. Microbiol.* **74**, 1459–1470 (2009).
30. Nano, F.E. *et al.* A *Francisella tularensis* pathogenicity island required for intramacrophage growth. *J. Bacteriol.* **186**, 6430–6436 (2004).
31. de Bruin, O.M. *et al.* The biochemical properties of the *Francisella* pathogenicity island (FPI)-encoded proteins IglA, IglB, IglC, PdpB and DotU suggest roles in type VI secretion. *Microbiology* **157**, 3483–3491 (2011).
32. Checroun, C., Wehrly, T.D., Fischer, E.R., Hayes, S.F. & Celli, J. Autophagy-mediated reentry of *Francisella tularensis* into the endocytic compartment after cytoplasmic replication. *Proc. Natl. Acad. Sci. USA* **103**, 14578–14583 (2006).
33. Golovliov, I., Sjöstedt, A., Mokrievich, A. & Pavlov, V. A method for allelic replacement in *Francisella tularensis*. *FEMS Microbiol. Lett.* **222**, 273–280 (2003).

ONLINE METHODS

Experimental setup. The silicon-based delivery chip was loaded onto a custom-built membrane pump for laser pulsing. The laser scanning system includes a Q-switched Nd:YAG laser (Minilite I, Continuum) with a wavelength at 532 nm, a pulse duration of 6 ns, and a beam diameter of 1 mm and is coupled with a 2D scanning mirror (Thorlabs) for rapid scanning across the entire active 1-cm^2 photothermal delivery area. After laser scanning, an external synchronized pressure source (FemtoJet, Eppendorf) is applied to deform the PDMS membrane to transfer cargo in the storage chamber into all cells on the platform. The setup for time-resolved imaging characterization is the same as Wu *et al.*'s research[19].

Cell culture on platform chips before BLAST. HeLa (ATCC), NHDF (Lonza) and RPTEC (Lonza) cells were routinely tested for mycoplasma using the Universal Mycoplasma Detection Kit (ATCC, 30-1012K) according to the manufacturer's protocol. Cells were seeded onto a clean chip 24 h before the BLAST procedure. Chips with HeLa and NHDF cells were placed in Dulbecco's modified essential medium (DMEM, Corning) supplemented with 10% (vol/vol) fetal bovine serum (FBS, Thermo Scientific) and 1% penicillin/streptomycin (Mediatech) and kept in an incubator at 37 °C and 5% CO_2. In the case of PB-MDMs, 0.01% poly(L-lysine) (Sigma) was coated on chips to improve cell adhesion. Peripheral blood mononuclear cells were isolated on Ficoll-Hypaque gradients, adjusted to 6×10^6 cells/ml in RPMI-1640 (Corning) supplemented with 200 mM L-glutamine, penicillin/streptomycin, and 20% autologous serum, and incubated for 3 d in sterile screw-cap Teflon wells (Savillex Corp.) at 37 °C, 5% CO_2. The PB-MDMs were washed, resuspended in RPMI 1640 with glutamine, penicillin/streptomycin and 10% (vol/vol) autologous serum and seeded onto the chip. After 90 min of incubation at 37 °C and 5% CO_2, the chip was washed to remove the nonadherent cells, and fresh culture medium was added for overnight incubation before use in experiments. These cells were obtained from a healthy donor and showed no evidence of mycoplasma infection by 4′,6-diamidino-2-phenylindole (DAPI) or Hoechst staining. Chips with RPTECs were placed in renal epithelial cell basal medium (REBM, Lonza) supplemented with 0.5% FBS and incubated at 37 °C and 5% CO_2.

Delivery materials. The total volume of the cargo storage chamber is 10 µl. *F. novicida* were grown in trypticase soy broth supplemented with 0.2% cysteine (TSBC), washed once with Hank's balanced salt solution (HBSS, Mediatech) and resuspended in HBSS to a final OD of 10.0 at 600 nm. *L. monocytogenes* were grown in brain heart infusion medium (BHI) at 30 °C to OD 1.0, washed once with HBSS and resuspended to OD 1.0. Green fluorescent polystyrene beads (20 nm, 200 nm, 500 nm, 1 µm and 2 µm) modified by carboxylate (FluoSpheres, Invitrogen) were suspended in phosphate-buffered saline (PBS) (Corning) at 10^{14}, 10^{11}, 10^{11}, 10^{10} and 10^{10} beads/ml, respectively. 200 nm red fluorescent magnetic beads (Chemicell) modified by streptavidin were diluted to 2×10^{10} beads/ml in PBS. Mouse anti–α tubulin with Alexa Fluor 488 (ab195887, Abcam) was prepared to 100 µg/ml in PBS. β-lactamase enzyme from *Enterobacter cloacae* (Sigma) was dissolved in PBS at 50 units/ml.

Delivery efficiency and cell viability. Cells with cargo inside were counted as delivered cells. Delivery efficiency, expressed as a percentage, was calculated as the number of delivered cells divided by the total number of cells × 100. Cell viability, expressed as a percentage, was determined by propidium iodide (5 µg/ml) staining 90 min after delivery and calculated as the number of the cells lacking red fluorescence divided by the total number of cells × 100.

Reproducibility information. Data on optimizing the performance of BLAST chips are means of at least five randomly selected fields of view with at least 438 cells counted per data point; error bars represent s.d. (**Fig. 2a–d**). Data on testing the transient window for large-cargo delivery are means of at least four randomly selected fields of view with at least 1,825 cells counted per data point; error bars represent s.d. (**Fig. 2e**). Data on testing the transient window for small-molecule delivery are means of at least three randomly selected fields of view with at least 351 cells counted per data point; error bars represent s.d. (**Fig. 2f**). Data regarding the 3-d cell viability test are means of at least five randomly selected fields of view with at least 1,057 (HeLa), 737 (NHDFs), 1,464 (PB-MDMs) or 387 (RPTECs) cells counted per data point; error bars represent s.d. (**Fig. 2g**). Data on cell proliferation after cargo delivery are means of at least five randomly selected fields of view with at least 780 (NHDFs), 1,569 (PB-MDMs) or 576 (RPTECs) cells counted per data point; error bars represent s.d. (**Fig. 2h**). Data on enzyme delivery are means of at least three randomly selected fields of view with at least 353 cells counted per data point; error bars represent s.d. (**Fig. 3**). Data on the intracellular localization and growth of *F. novicida* after BLAST are means of at least seven randomly selected fields of view with at least 74 cells counted per data point; error bars represent s.e.m. (**Fig. 5**). Data on delivery efficiency and cell viability after delivery of different polystyrene beads are means of at least four randomly selected fields of view with at least 562 cells counted per data point; error bars represent s.d. (**Supplementary Fig. 4d**). No sample-size estimates were performed to ensure adequate power to detect a prespecified effect size.

Bacterial and cell culture. *F. novicida* Utah 112 was grown in TSBC or on chocolate agar. When needed, kanamycin and hygromycin were included in the *F. novicida* cultures at 20 µg/ml or 200 µg/ml, respectively. *L. monocytogenes* was grown in BHI medium. When needed, streptomycin and erythromycin were included in the *L. monocytogenes* cultures at 200 µg/ml and 5 µg/ml, respectively. Human monocytic cell line THP-1 (ATCC TIB202) was maintained in RPMI-1640 supplemented with 10% FBS and penicillin (100 IU)/streptomycin (100 µg/ml) and confirmed as being free of mycoplasma by using the Universal Mycoplasma Detection Kit (ATCC). Prior to infection, THP-1 cells were differentiated with 100 nM phorbol 12-myristate 13-acetate for 3 d. Bacteria were pre-opsonized by incubation in 10% human serum type AB in HBSS at 37 °C for 10 min, spun onto THP-1 macrophages at 800*g* for 30 min at 4 °C, and incubated at 37 °C for 30 min to allow uptake. The infected monolayers were treated with 10 µg/ml gentamicin in DMEM containing 10% FBS for 30 min, washed and incubated in DMEM containing 10% FBS and 0.1 µg/ml of gentamicin. At specified time points, the infected monolayers were lysed with 1% saponin

in PBS for 5 min, and the serial diluted lysates were plated on chocolate agar for bacterial CFU enumeration.

Actin phalloidin staining. NHDFs were seeded onto BLAST chips as described above. *L. monocytogenes-GFP* Δ*hly* Δ*plcB* (green), strain 10403S, was delivered by BLAST with (or as a sham control) without laser pulsing. The NHDF cells were washed, incubated at 37 °C for 6 h in DMEM with 10% FBS and 5 μg/ml gentamicin (which kills any residual extracellular bacteria) and fixed in 4% paraformaldehyde in PBS. F-actin was stained with phalloidin-rhodamine (Molecular Probes) according to the manufacturer's protocol.

Generation of Δ*iglC* and green fluorescent *F. novicida* strains. *F. novicida* was chemically transformed with the suicide plasmid pMP590-Δ*iglC*-ExC to generate an unmarked in-frame deletion mutant of *iglC* by allelic exchange. The resulting kanamycin-resistant clones with plasmid integration were counterselected on chocolate agar containing 5% sucrose for loss of the integrated plasmid. The clones that were resistant to sucrose and sensitive to kanamycin were screened for deletion of the *iglC* gene by PCR and western immunoblotting analyses. GFP-expressing *F. novicida* strains were generated by introducing pMP633 carrying a codon-optimized superfolder *gfp* (sfGFP; F.E. Nano, University of Victoria) driven by the bacterioferritin (FTL_0617) promoter. For complementation of *iglC*, pMP633BC-*iglC*-sfGFP was introduced into *F. novicida* Δ*iglC* for bicistronic expression of *iglC* and sfGFP. Bacterial strains, plasmid constructs and primers used in this study are listed in **Supplementary Table 2**.

Digitonin permeabilization assay. Vacuolar versus cytosolic localization of bacteria was assessed by a modification of the differential digitonin permeabilization method of Checroun *et al.*[32], which permeabilizes plasma membranes but not bacterial vacuoles. After BLAST delivery of bacteria into HeLa cells, the monolayers were allowed to recover for 30 min; stained for 10 min with 20 μg/ml Alexa-Fluor 647 WGA (Molecular Probes); washed with HBSS; fixed for exactly 1 min with 4% paraformaldehyde in HBSS; permeabilized for exactly 1 min with 0.05 mg/ml digitonin in 110 mM potassium acetate, 20 mM HEPES, 2 mM $MgCl_2$ and 15% sucrose (KHM with 15% sucrose); washed twice with KHM containing 15% sucrose; incubated with chicken anti–*F. novicida* antibody[34] (1:1,000 dilution, a gift from D.M. Monack, Stanford University), in KHM buffer containing 15% sucrose and 0.1% BSA; washed three times with KHM containing 15% sucrose; fixed for 30 min in 4% paraformaldehyde in 75 mM sodium phosphate, pH 7.4; permeabilized thoroughly with 0.1% saponin in PBS; washed with PBS; and incubated with Texas red-X–conjugated goat anti-chicken antibody (1:50 dilution, ab6875-1, Abcam) for 90 min at room temperature. Monolayers were incubated with DAPI (1 μg/ml), washed with PBS and viewed by fluorescence microscopy. Green fluorescent bacteria within the WGA-stained host cell borders that stained by the red antibody probe were scored as being cytosolic, and those that were not stained by the red fluorescent antibody probe were scored as being membrane bound (vacuolar) (**Supplementary Fig. 9**).

Imaging. Fluorescence images were obtained using an inverted fluorescence microscope (Axio Observer.D1m, Carl Zeiss) with 10× and 40× objective lenses. Scanning electron micrographs were taken by a field emission scanning electron microscope (Hitachi S4700). Confocal images were captured using a laser scanning confocal microscope (SP2 AOBS, Leica).

34. Jones, J.W. *et al.* Absent in melanoma 2 is required for innate immune recognition of *Francisella tularensis*. *Proc. Natl. Acad. Sci. USA* **107**, 9771–9776 (2010).

doi:10.1038/nmeth.3357